SAXS Investigations on Uniaxially Drawn Fibers Obtained from Polyethylene Reactor Powder

Stefano Ottani,[†] Elena Ferracini,[†,‡] Adele Ferrero,[†,‡] Viscardo Malta, and Roger S. Porter*[,§]

Centro di Studio per la Fisica delle Macromolecole del C.N.R., Via Selmi 2, 40126 Bologna, Italy, Dipartimento di Chimica "G. Ciamician", Università di Bologna, Via Selmi 2, 40126 Bologna, Italy, and Polymer Science and Engineering Department, University of Massachusetts, Amherst, Massachusetts 01003

Received August 28, 1995; Revised Manuscript Received January 12, 1996[⊗]

ABSTRACT: The polyethylene powders studied were synthesized by both slurry and gas-phase processes at temperatures ranging between 30 and 85 °C. Fibers were drawn from these nascent powders under identical processing conditions. The maximum achievable draw ratio was found to be strongly dependent on synthesis conditions. Highest ductilities are obtained for samples synthesized by a slurry process at 85 °C. Small-angle X-ray scattering (SAXS) measurements were performed on fibers coextruded from reactor powders at a draw ratio of 6. No interferential effects were detected in the equatorial profiles. In contrast, the meridional SAXS patterns display interference peaks whose intensities bear definite relationships to both ductility and synthesis conditions. Fibers obtained from samples synthesized by a slurry process at 85 °C display a well-defined interference peak along the meridional direction. Fibers obtained from samples synthesized in the other conditions show only an ill-defined broad shoulder. Results of peak profile analysis show that higher peak intensities and larger peak widths are obtained for most ductile samples. According to the Peterlin model for draw, these trends are ascribed to different contents of taut tie molecules. Changes in the crystallization dynamics produced by different synthesis conditions are discussed for their effect on the amount of taut tie molecules.

Introduction

High and ultrahigh molecular weight polyethylene (HMWPE) can be uniaxially drawn to high draw ratios by different methods. These polymers can be drawn either after solubilization or in the solid state. The processing techniques are commonly subdivided into gel-spinning methods[1] and solid-state extrusion (SSE).[2] Ultradrawn high-modulus fibers can be obtained by each method. The macroscopic draw of high polymers has been related to the extension of the transient network formed by the macromolecules, with entanglements acting as friction centers or temporary nonlocalized junctions.[2−4] According to this model, the achievement of high draw ratios has been ascribed either to the ability of the drawing method to release constraints in the entangled network (gel spinning) or to the low entanglement density of the specimen for draw, both coupled with the high ability of polyethylene (PE) crystals to rearrange on draw.[2,4−8] For SSE methods, nascent reactor powders provide less entangled morphologies, resulting from crystallization directly on synthesis.[2,7,9]

The present study is part of a general effort to relate synthesis parameters to the ductility of reactor powders, with the purpose of obtaining an optimal set of synthesis conditions leading to highest ductilities. Several techniques have been used to investigate effects of synthesis on properties of reactor powders. Results by differential scanning calorimetry (DSC)[10] and Raman longitudinal acoustic mode (LAM)[11,12] show that synthesis has important effects on nascent crystallinity and on the interphase, the region between the crystal and the amorphous phase, where entanglements are located.[13] Experiments show that higher nascent crystallinities and lower interfacial contents correspond to higher values of the maximum achievable draw ratio of the nascent reactor powders.[12,14]

In this study, the structural changes induced in several HMWPE samples have been tested at each draw step by small-angle X-ray scattering (SAXS). In the first part of this work,[14] SAXS patterns were recorded for the first two steps of the procedure, that is for nascent reactor powders and subsequent compression-molded (sintered) plates. These SAXS profiles were analyzed according to the generalized Guinier approximation,[15] for which the results are consistent with a maximum of five dimensional groups in the globular particles. Several relationships between the sizes and the mass fractions of these dimensional groups and the synthesis conditions have been identified. Estimates of the changes related to segmental chain mobility have been obtained by comparing differences between reactor powders and the corresponding sintered plates. Attention here is focused on the SAXS analysis of uniaxally drawn samples of PE. The reactor powder grains are first compacted and then coextruded under pressure into a fiber, which is the starting point for further draw in free space.[2] Deformations of the nascent structures involve first the intercrystalline regions, which are the most ductile portions of the morphologies.[16−21] Chain segments in the crystalline cores require greater extensions to be unfolded and re-formed into the growing fiber. Comparisons between SAXS patterns of sintered samples and of the corresponding coextruded fibers can reveal the structural changes stemming mainly from the drawing of the soft intercrystalline material and from the associated deformations in the crystallite fold surfaces. Understanding the relationships between synthesis conditions and the nature of this transformation is of special relevance for the tailoring of the ideal set of synthesis parameters to obtain ultradrawable nascent reactor powders of PE.

[†] Centro di Studio per la Fisica della Macromolecole del C.N.R.
[‡] Università di Bologna.
[§] University of Massachusetts.
[⊗] Abstract published in *Advance ACS Abstracts,* March 15, 1996.

0024-9297/96/2229-3292$12.00/0

Table 1. Coextruded Polyethylenes: Processing Conditions and Peak Parameters from Meridional SAXS Patterns

sample identification	T (°C)		EDR	TDR_{max} (135 °C)[a]	tensile modulus (GPa)	integrated intensity[b]	fwhm[c]	$\bar{L}$ (Å)
	sintering	coextrusion						
Sl30-05.9	128	120	5.7	9		2.59	0.98	511
Sl30-12.4	122	119	5.7	6		1.94	0.82	465
Sl85-00.3	126	120	5.6	50	49	4.91	1.07	394
Sl85-02.0	127	120	5.7	85	57	6.56	1.24	384
Sl85-04.8	122	120	5.8	98	75	4.87	1.12	396
Gp30-01.9	120	120	7.0	7		1.01	0.77	436
Gp85-00.2	124	121	5.8	19		1.61	0.82	386
Gp85-01.0	120	120	5.8	22		1.00	1.00	346

[a] TDR_{max}, the maximum total draw ratio, is EDR, the extrusion draw ratio, multiplied by the second-stage free-space tensile draw ratio. Values of TDR_{max} were obtained under optimal conditions by drawing coextruded samples whose initial EDR ranged from 6 to 8.[22] [b] Peak integrated intensities expressed as fractions of the reference sample Gp85-01.0. [c] Peak full widths at half-maximum expressed as fractions of the reference sample Gp85-01.0.

Experimental Section

HMWPE samples were synthesized by Union Carbide Corp., using Ziegler−Natta heterogeneous catalysis, by either slurry or gas-phase process. Details of the syntheses have been given.[10] *n*-Hexane was used as monomer solvent in the slurry process. For both gas-phase and slurry syntheses, ethylene pressure was 230 psi at 30 °C and 100 psi at 85 °C. Samples have been classified by synthesis process type, synthesis temperature, and molecular weight according to the pattern Ss*tt*-*mm.m*, where Ss is the synthesis type, *tt* the synthesis temperature, and *mm.m* the molecular weight. Thus Sl30-02.9 stands for a sample synthesized by a slurry process at 30 °C, having molecular weight, $\bar{M}_v$, equal to 2.9×10^6.

Plates 1 mm thick were prepared by pressing powders at 150 kg cm^{-2} under vacuum for about 8 h. Processing temperatures ranged between 120 and 128 °C. Some difficulties were encountered in setting and maintaining uniform processing temperatures. However, sintering temperatures were kept at least 10−15 °C below the previously measured DSC melting peak temperatures. Strips (4 mm wide) cut from the compressed plates were inserted between the two halves of a cylindrical split billet of high-density PE and coextruded through a bronze conical die of 20° entrance angle. The extrusion draw ratio (EDR) was kept between 5 and 6, as measured from the displacement of ink marks preimprinted on the strip surface. Coextrusion temperature was 120 °C. These process conditions stem from a compromise between the need of preserving as much as possible of the undeformed nascent structure and the requirement of a quality (porous free) starting sample for the second-stage drawing. Another set of fibers was also coextruded at EDR ranging from 6 to 8. This range was found to provide optimal starting points for the second-stage draw.[22] Values of the maximum total draw ratio (TDR_{max}) reported in this work were obtained from this second set of extrudates[22] as the product of the draw ratios in the two steps.

Samples have been investigated by a high-resolution Kratky camera (Compact) with Cu Kα radiation. Intensities were measured by a proportional counter with pulse height discriminator. Slit widths for all the scans were 80 μm for the entrance slit and 200 μm for the counter slit Intensities were recorded for **b** ($|\mathbf{b}| = b = 2 \sin \theta/\lambda$) ranging from 9.5×10^{-4} to 3.5×10^{-2} Å^{-1}. Desmearing of intensity profiles was performed by Vonk's method.[23] SAXS patterns of coextruded samples were recorded on both the equatorial and the meridional directions, that is, along directions normal and parallel to the fiber axis, respectively. Orientation of the microdomain was controlled by wide-angle X-ray scattering (WAXS) using a flat-film camera. Relevant data on sample characterization and processing conditions are reported in Table 1.

Results and Discussion

1. Guinier Analysis of the Equatorial Profiles. SAXS equatorial profiles of coextruded fibers show no detectable interference. These profiles have been analyzed by an iterative generalized Guinier approximation.[15] As reported,[24] this method can be successfully applied to condensed systems, like polymer fibers, provided that effects of interparticle interference are negligible. According to the structural model of Bonart and Hosemann,[15,24] the fiber structure can be approximated as a complex assembly of microfibrillar units. Accordingly, values of the radii of the particle cross-sections can be computed from the equatorial profiles,[24] while the particle lengths can be obtained from the meridional profiles. The iterative Guinier analysis of the equatorial patterns was performed by applying the same method used to investigate the corresponding nascent reactor powders.[14] The adjustable parameters of a model function were optimized by least squares fitting to the desmeared SAXS profiles. This model function was made up by a summation of Gaussian functions[24,25] plus a constant background to account for the liquid-like scattering.[26] By the Guinier approximation, every Gaussian peak represents the contribution of a group of particles to the total scattering.

In the equatorial direction, the Gaussian components of the model function in the two-dimensional approximation[15] are given by

$$I_i(b) = I_i(0) \exp(-2\pi^2 b^2 R_{gi}^2) \tag{1}$$

where R_{gi} is the electronic radius of gyration of the cross-section of the *i*th dimensional group of rodlike particles. The corresponding cross-section radius is given by $R = 2^{1/2} R_g$. Values of R_{gi} and $I_i(0)$ were least-squares adjusted to obtain the best fit to the data. The best fit was achieved by summing the contributions of four Gaussian functions plus a constant background. Figure 1 reports results of the analysis of a typical equatorial scan.

The weight distribution function, $W(R)$, of the dimensional groups defined above is related to the scattered intensities as follows:[27]

$$I(b) = C \int_0^\infty W(R) R^2 \exp(-2\pi^2 b^2 R_g^2)\, dR \tag{2}$$

where C is a constant. For a finite number of groups, extrapolation of intensities to $b = 0$ gives

$$I(0) = \sum_i W_i(R_i) R_i^2 \tag{3}$$

Values of $I_i(0)$ and R_i, obtained by least squares, can be introduced in eq 3 to compute the percent mass fractions of the corresponding dimensional groups, wt % (R_i). Values of R_i and wt % (R_i), obtained from the equatorial profiles, are reported in Table 2.

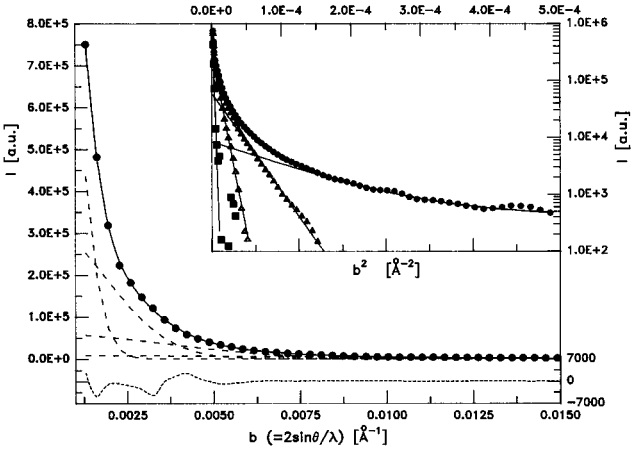

Figure 1. Guinier analysis of the equatorial profile of the Gp85-01.0 fiber: (●) experimental points; (—) least squares fit; (- - -) individual Gaussian components of the least squares fit; (···) difference curve (=experimental − least squares fit). To enhance visibility, the *y* scale of the difference curve has been enlarged. On the top-right corner, the same results are reported in terms of the well-known Guinier plot.

Table 2. Coextruded Polyethylene Fibers: Guinier Analysis of Equatorial SAXS Patterns

	Average Radii of Particle Cross-Sections			
sample identification	R_1 (Å)	R_2 (Å)	R_3 (Å)	R_4 (Å)
Sl30-05.9	34	70	134	273
Sl30-12.4	34	65	129	262
Sl85-00.3	36	73	138	305
Sl85-02.0	33	64	123	254
Sl85-04.8	35	68	134	307
Gp30-01.9	35	66	141	361
Gp85-01.0	35	71	136	328
	Average Mass Fractions of Dimensional Groups R_i			
sample identification	wt % (R_1)	wt % (R_2)	wt % (R_3)	wt % (R_4)
Sl30-05.9	32	31	23	14
Sl30-12.4	30	37	22	11
Sl85-00.3	40	34	21	5
Sl85-02.0	35	35	23	7
Sl85-04.8	33	37	23	7
Gp30-01.9	32	26	24	18
Gp85-01.0	35	31	24	10

Results of previous investigations on the samples in Table 1 show that the reactor powders are organized as polydisperse systems of globular particles.[14] Polydispersity in globule dimensions is such that several chain-folded crystallites may group to form larger globular clusters. SSE provides the first appearance of interferential effects in the meridional profiles, which should correspond to the rearrangement of nascent globular clusters into aggregates of higher regularity. The significance of these rearrangements can be estimated from the values of particle dimensions and weight fractions in Table 2 and from comparisons of the globule average radii at the several processing stages reported in Table 3.

Along the equatorial direction, a relationship among particle dimensions of each fiber can be obtained from R_i values in Table 2. Independently of the synthesis parameters, radii of the higher dimensional groups are close multiples of 35 Å, that is, the radius of the smallest group. Such a pattern and the presence of a long period distance in the meridional direction (Figure 2a,b) suggest that significant parts of these systems are organized in bundle-like fibrillar aggregates (see Figure 3), whose basic unit has a diameter of ≅70 Å.[24] Bundles

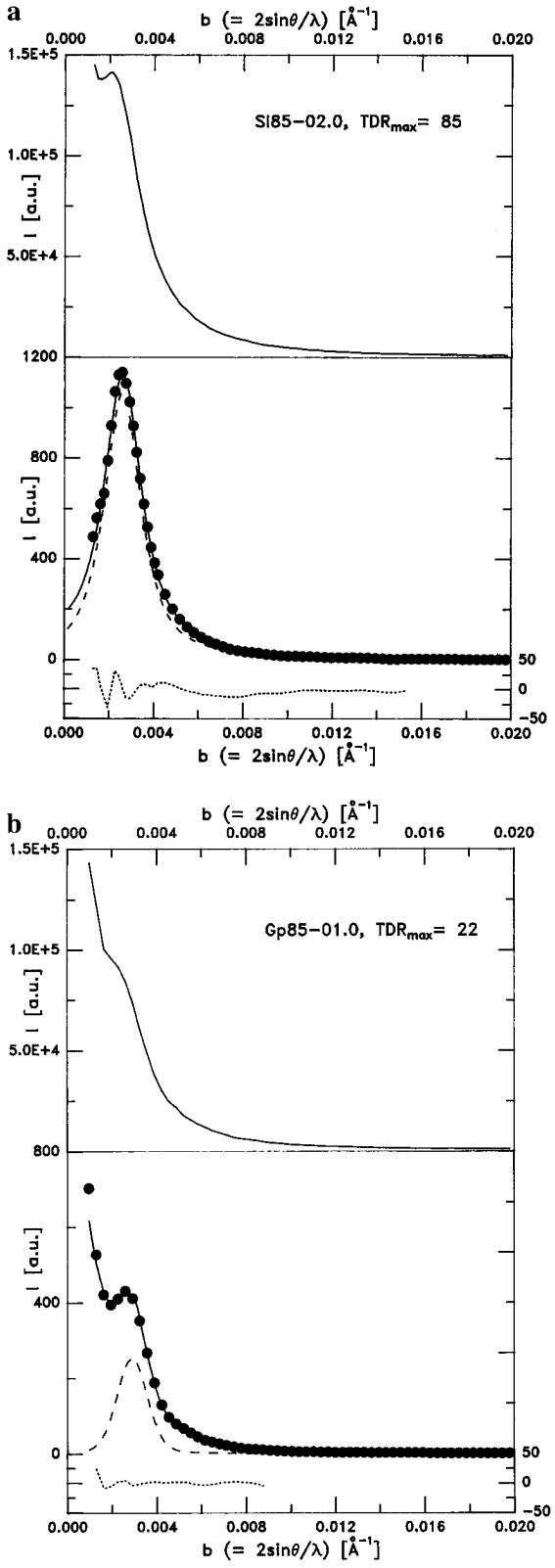

Figure 2. (a) Meridional scans of SAXS patterns of Sl85−02.0 coextruded fiber. Intensities are in arbitrary units. Top: (—) experimental profile. Bottom: (●) desmeared intensities; (—) least squares fit to desmeared intensities. (- - -) peak component of the least squares fit; (···) = difference curve (=desmeared − least squares fit). (b) Meridional scans of SAXS patterns of Gp85-01.0 coextruded fiber. Intensities are in arbitrary units. Symbols and line types as in (a).

of 4, 16, and 64 or 100 fibrils may be compatible with radii of 70, 140, and 280 or 350 Å, respectively, as can be deduced from the values reported in Table 2 for the four dimensional groups. Data in Table 3 show that the

Table 3. Changes in Particle Dimensions with Processing

process type	processing temp (°C)	R_1 (Å)	R_2 (Å)	R_3 (Å)	R_4 (Å)	R_5 (Å)
		Sample Sl30-05.9				
nascent powder[a]	30	23	36	67	138	328
sintered plate[a]	128	30	48	76	153	315
coextruded fiber (SAXS equatorial)[b]	120	34		70	134	273
		Sample Sl30-12.4				
nascent powder[a]	30	24	36	64	133	323
sintered plate[a]	122	33		70	151	320
coextruded fiber (SAXS equatorial)[b]	119	34		65	129	262
		Sample Sl85-02.0				
nascent powder[a]	85	28	55	99	224	456
sintered plate[a]	127	33	56	87	167	322
coextruded fiber (SAXS equatorial)[b]	120	33	64		123	254
		Sample Gp85-01.0				
nascent powder[a]	85	26	41	74	132	326
sintered plate[a]	120	31		65	140	347
coextruded fiber (SAXS equatorial)[b]	120	35		71	136	328

[a] See ref 14 for a discussion on R_i of reactor powders and sintered plates. [b] In this table, the R_i labeling of dimensional groups reported in Table 2 has been changed to facilitate comparisons between the corresponding coextruded fibers and sintered specimens.

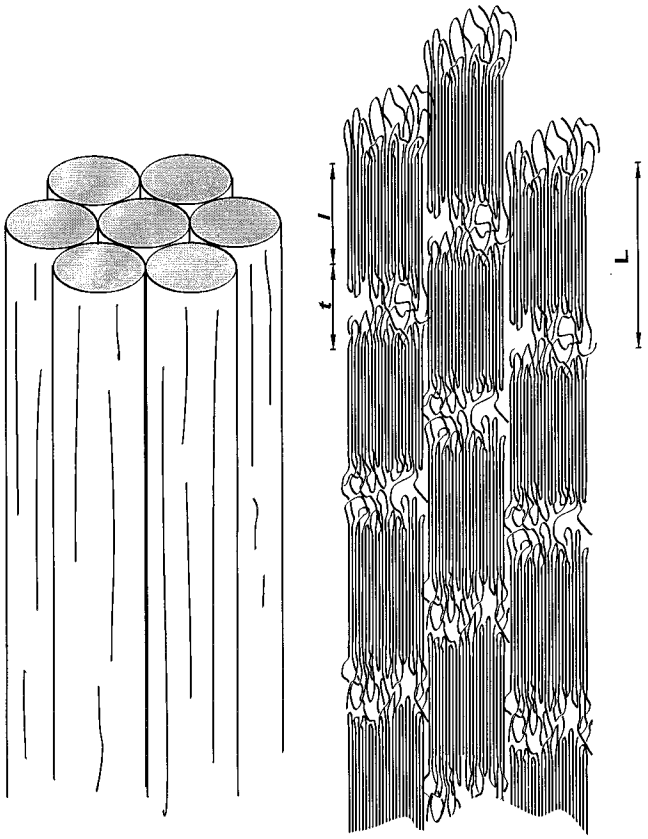

Figure 3. Bundle-like aggregates of microfibrils according to the Hosemann−Bonart model. On the right, cross sections of bundles are displayed. L is the long period repeat distance, and l and t are the crystalline and the intercrystalline layer thicknesses, respectively.

smaller dimensional groups of the coextruded fibers do not change significantly from the corresponding sintered plates. In contrast, the radius of the largest group undergoes a significant reduction on draw, at least in samples synthesized by a slurry process.

Another interesting effect of synthesis conditions on the formation of the bundle-like fibrillar aggregates can be found via the weight fractions in Table 2. These data show that, for ductile Sl85 samples, the weight fraction of the largest bundle-like aggregates is lower. Thus, despite their higher ductilities, these samples do not readily coalesce on draw into large fibrillar structures. This behavior is not well understood. In fact, the discussion of the influence of synthesis conditions on the dimensional changes of the largest dimensional groups requires a detailed knowledge of the inner structure of the nascent aggregates and of their deformation. What should be found first is whether the largest nascent globules possess multiglobular structures, like those obtained by clusters of small crystallites. In this case, the energy to overcome the binding forces among distinct globules would not be high. In contrast, higher energies are required if the deformation involves the shear buckling of thick crystalline lamellae embodied in the largest nascent aggregates.

Data in Tables 2 and 3 and in Figure 2a,b support the conclusion that draw transforms most of the nascent globular aggregates into fibrillar clusters whose cross-section is a function of the number of bundled fibrils. Figure 3 illustrates the relationship between crystallites and fibrils.[24] In the equatorial profiles, interference effects are not detected. This can be ascribed to the absence of ordered repeating patterns across the fiber and justifies the use of the generalized Guinier approximation.

2. Peak Intensities and Synthesis Conditions. According to the two-phase model,[28] intensities in the SAXS patterns of polymers are a function of $\langle\Delta\rho^2\rangle$, the mean squared electron density fluctuations between the crystalline and the noncrystalline phases along the X-ray beam path. The presence of a sharp interference peak is strictly related to phase ordering, since interference is attributed to the regular stacking of chain-folded crystalline lamellae and amorphous interlamellar layers.[29,30] An important feature of this idealized picture, reported in Figure 3, is the constancy of the long period, L, given by the sum of l, the lamellar fold length, and t, the thickness of the amorphous interlamellar layer. Average values of the long period, $\bar{L}$, can be measured directly from the angular position of SAXS interference peaks, while l and t are obtained indirectly.[31−33] Interference peaks are a characteristic feature of SAXS profiles recorded from melt-crystallized samples.[29,30,34] Studies on the draw of melt-crystallized samples show that intensities of such peaks are stronger in the first stage of draw, decreasing as draw ratio is increased.[16,35] In contrast, no interference can be detected in SAXS patterns of nascent reactor powders and in those of the corresponding sintered plates.[14] The absence of such interferential effects might be attributed to thick nascent crystallites or even to chain-extended crystals,

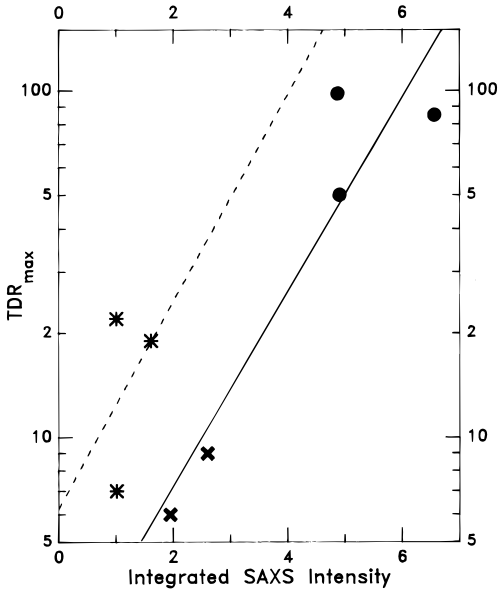

Figure 4. Peak integrated intensity fractions *vs* TDR_{max}. Fractions were computed by dividing each integrated intensity by the Gp85-01.00 intensity value. (●) Sl85 samples; (×) Sl30 samples; (*) Gp samples; (—) least squares fit to slurry samples; (- - -) least squares fit to gas-phase samples.

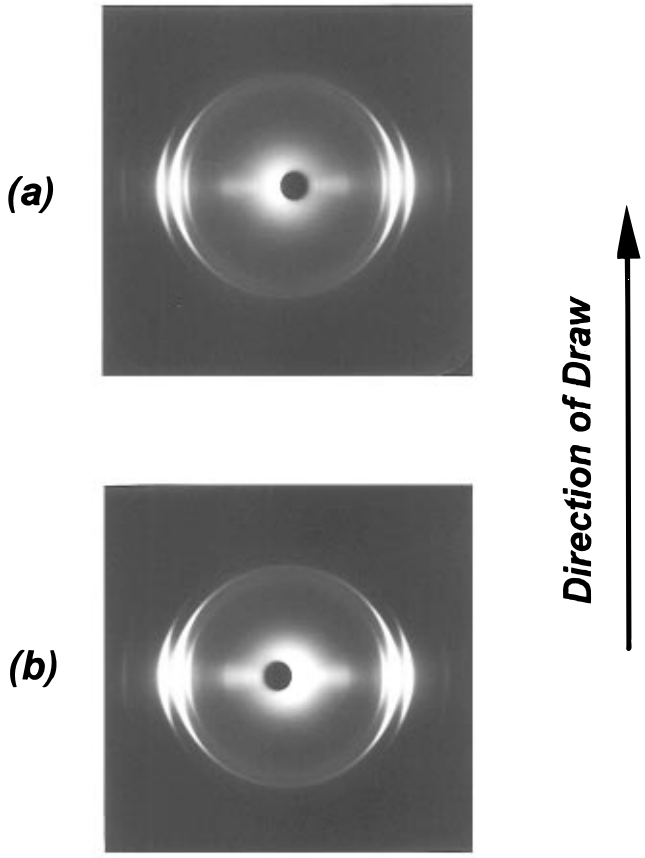

Figure 5. (a) Flat-film X-ray photograph of the Sl30-05.9 coextruded fiber. (b) Flat-film X-ray photograph of the Sl85-02.0 coextruded fiber. Fiber axis is along the page.

which would have shifted SAXS interference peaks below the experimentally accessible angular range. However, this hypothesis is not supported by data on nascent crystallite thicknesses calculated from the DSC melting temperatures[10] and by Raman LAM,[11] which give values in the range 200−350 Å. Such values are well within the instrumental limits of the Kratky camera used. Thus, it is concluded that the absence of interference in reactor powders can be ascribed to the irregular crystallite stacking in the nascent globular clusters. However, parts a and b of Figure 2 show that, after the first draw step, the meridional profiles display interference peaks whose intensities vary with synthesis conditions. The appearance of an interference peak in the drawn fiber can be attributed to the increased regularity of $\bar{L}$, induced by transformation of the globular aggregates into the bundle-like fibrillar structures. The patterns in Figure 2a,b illustrate a relationship between the SAXS profiles and synthesis parameters, which holds for all the samples tested. Samples synthesized by a slurry process at 85 °C display well-defined interference peaks along the meridional spectrum. Samples synthesized in the other conditions show only an ill-defined broad shoulder.

The dependence of peak intensities on synthesis conditions was investigated by peak profile analysis. Intensities of the meridional SAXS patterns of samples listed in Table 1 were preliminarily desmeared and scaled to a common reference sample (Gp85−01.0). SAXS profiles were analyzed by fitting an adjustable function to the initial portion of the experimental curve.[35] This function was computed as the sum of a pseudo-Voigt peak function,[36] *viz.* a linear combination of a Gaussian with a Lorentzian, plus a polynomial to account for the underlying continuous scattering. Analysis of the interferential component of the meridional scattering is reported in Table 1 and Figure 4. The structural changes produced by the coextrusion process are dissimilar, albeit processing conditions and final draw were similar for all samples investigated. Figure 4 shows that peak intensities of Sl85 samples are systematically high and correspond to high values of the final TDR_{max}. This trend cannot be attributed to differences stemming from the orientation of the crystalline microdomains in fibers obtained from different reactor powders. In fact, the WAXS flat-film photographs in Figure 5 show that the degree of orientation of different fibers is substantially the same, as expected for identical EDRs.

3. Peak Broadening and Synthesis Conditions. Peak broadening was evaluated from the pseudo-Voigt[36] function as the full width at half-maximum (fwhm). The corresponding fractions obtained by dividing each fwhm by the value of the Gp85-01.00 sample are plotted in Figure 6 *vs* the corresponding TDR_{max}. The straight line in this figure reports the result of a least squares fit. With this correlation, samples group according to their synthesis conditions. On top are the Sl85 samples, which display the highest ductility. The Gp85 samples are intermediate, while samples synthesized at 30 °C show the lowest values of TDR_{max} and fwhm, independent of the synthesis type.

Peak broadening can be attributed to two structural parameters: the regularity of the lamellar stacking, that is the paracrystalline fluctuations in the long period, L, and the length of the coherently diffracting domains of stacked lamellae (see Figure 3). Shorter domains and larger fluctuations will correspond to larger peak widths. If paracrystalline fluctuations can be neglected, domain lengths can be evaluated by fwhm values. However, investigations on the mesoscopic structure of nascent reactor powders[14] showed that irregularities in the lamellar stacking and fluctuations in the long period are both significant. Experimental evidence for the presence in these nascent systems of well-formed crystalline lamellae was obtained by both

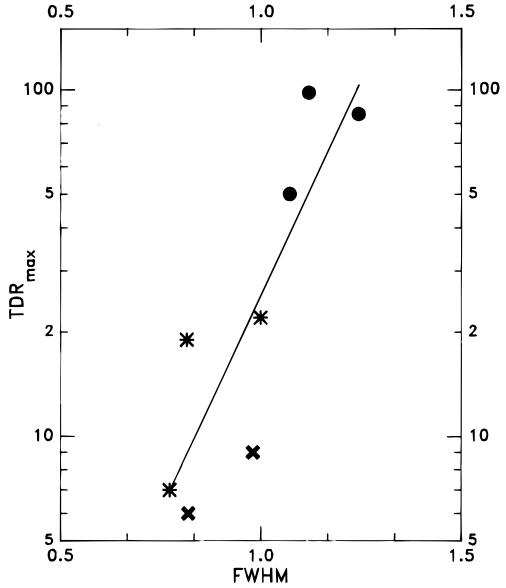

Figure 6. Peak full width at half-maximum fractions *vs* TDR_{max} fractions were computed by dividing each fwhm by the value of the Gp85-01.00 sample. Symbol coding as in Figure 4. (—) least squares fit to data.

DSC and Raman LAM.[10−12] In contrast, no interference effect was detected in the SAXS patterns of reactor powders. This was ascribed to the irregular stacking of crystal lamellae. In fact, the large amount of interparticle voids in these nascent systems[14] can increase the stacking disorder, by increasing irregularities in the thickness of the interlamellar layers, *t*. Parts a and b of Figure 2 show that the mesoscopic structure of coextruded fibers is still affected by synthesis conditions. Thus, contribution of nascent interparticle voids to the fiber stacking disorder can be important. In these conditions, fwhm values do not provide accurate estimates of the length of coherently diffracting domains.

A global inspection of data in Figures 4 and 6 leads to the following conclusions: higher drawabilities are obtained with samples that, upon draw, display less defined microfibrillar structures. In fact, samples synthesized at 85 °C by a slurry process display higher peak intensities and larger peak widths. Such a combination of synthesis conditions, peak intensities, and peak widths corresponds also to higher values of TDR_{max}

4. Effects of Synthesis Conditions on Powder Ductilities and on the Mesoscopic Structures of Coextruded Fibers. Several molecular models rationalize the behavior of high-modulus fibers.[16−21] The one proposed by Peterlin,[16,17] and reported in Figure 7, provides a satisfactory description of the draw of PE, especially at low-to-medium draw ratios. By this model, blocks of folded chains are extracted from the tilted crystallites (the white zone in Figure 7) and incorporated into the growing fibril (the dark gray zone). Interconnections among the crystalline blocks become taut tie molecules which concentrate in the intercrystalline regions (the medium-gray zones in Figure 7). At low draw, microfibrils are considered to be the structural elements directly responsible for fiber properties. In fact, the longitudinal strength results from the partially extended tie molecules and their periodicity along the fiber axis via the alternating crystalline and noncrystalline regions.[16] In the initial stage of the draw, chain-folded crystallites are dominant.[37,38] As drawing proceeds, more chain extension occurs. At high draw, microfibrils disappear[37] and an almost continuous crystalline phase is formed. Transmission electron microscopy has shown that the basic unit of this continuous structure is a protofibril,[38] where large portions of the core material are chain-extended crystals with small chain-folded crystalline blocks distributed along this core.[38] All the above-mentioned models relate the decrease in SAXS peak intensity to the reduction of $\langle\Delta\rho^2\rangle$ between crystalline and noncrystalline regions as draw is increased.[16,35,39] In ultradrawn PE, SAXS interference peaks disappear following the annihilation of any stacked lamella structure.[38]

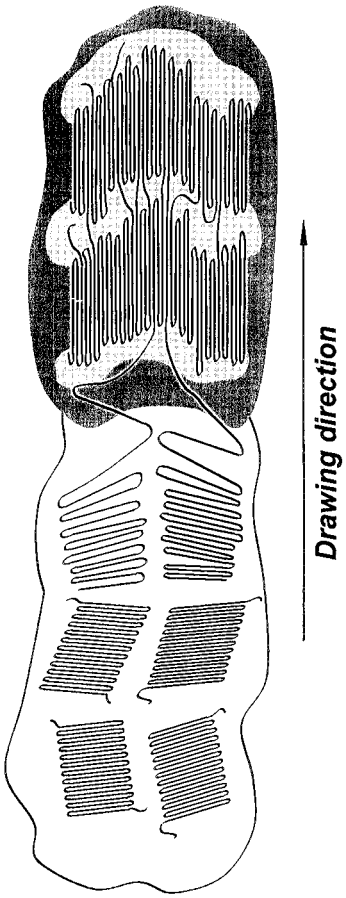

Figure 7. Schematic of the drawing process according to Peterlin.[16,17] Higher densities correspond to darker shadings.

As reported in Figures 2a,b and 4, fibers of the same draw, obtained from different reactor powders, display significant differences in $\langle\Delta\rho^2\rangle$ that can be attributed only to effects stemming from different synthesis conditions. Samples synthesized by a slurry process at 85 °C display meridional SAXS patterns typical of low draw ratios. For all the other synthesis conditions, SAXS patterns indicate that the intercrystalline regions are more strained. Thus, the same uniaxial draw corresponds to different chain deformations. Such molecular draw and the corresponding increase of taut tie molecules are larger for samples synthesized in the gas phase or by a slurry process at 30 °C. Moreover, comparisons with values of TDR_{max} show that larger initial amounts of taut tie molecules correspond to lower sample ductilities. These observations provide a correlation between synthesis conditions and values of TDR_{max} and lead to the conclusion that more strained initial intercrystalline regions significantly reduce sample ductilities.

Peterlin's model can also provide the basis to discuss the relationship between values of the fwhm and

TDR_{max} reported in Figure 6. Higher contents of tie molecules can lead to a distribution of the drawing stress among the different intercrystalline layers, providing a more uniform deformation. By increasing regularity in the values of l and t (Figure 3), higher uniformity in $\bar{L}$ can be obtained. Thus, a more stressed interphase in the first stage of draw may increase both the lengths of the coherently diffracting domains and the regularity of the long period. The same interphase effect can explain the relationship between synthesis conditions and values of the weight fractions obtained from the equatorial profiles and reported in Table 2. Samples of lower ductilities display higher weight fractions of the large bundles of fibrils.

Such correlations between ductilities and different amounts of taut tie molecules and strained chain arrangements can be discussed in terms of the influence of synthesis conditions on the degree of entanglement of nascent polymer powders. Wunderlich's principles of crystallization on synthesis[40] have been successfully employed to explain the effect of synthesis temperature on the crystallization dynamics and on the nascent degree of entanglement.[41] According to these principles, supercooling enhances the crystallization rate and simultaneously reduces the polymerization rate.[40] Then, crystallization on synthesis at high undercooling leaves shorter times for the growing chain segments to hang loose before being absorbed on the crystal surface. Thus, the probability of entanglement formation is reduced. In contrast, at high synthesis temperatures, polymerization and crystallization become practically independent processes. Polymer segments spend longer times in the molten state and chances to form new entanglements increase. Thus, according to this model, samples synthesized at low temperature should have low degrees of nascent entanglements. Several experimental confirmations have been reported.[7,41,42] However, such a conclusion does not agree with data reported in Table 1 and Figure 4, which show that, for both gas-phase and slurry processes, ductilities increase as synthesis temperature is increased. In contrast, the relationships among synthesis conditions, entanglements, and ductilities are confirmed: structural parameters related to entanglements, such as nascent crystallinities,[10,14] nascent interphase contents, and the amounts of taut tie molecules[12,16] display a defined correlation with powder ductilities.

Nonetheless, Wunderlich's correlation between synthesis and crystallization dynamics can provide a satisfactory explanation of the different type of dependence of TDR_{max} on SAXS peak intensities for the synthesis processes, reported in Figure 4. The full and dashed lines in this figure correspond to results obtained by linear least squares regressions for the two types of synthesis: slurry (full line) and gas phase (dashed). It can be seen that the two straight lines have quite similar slopes and that, along each line, higher drawabilities correlate with higher synthesis temperatures. Analysis of the trends corresponding to the dashed and solid lines in this figure leads to the conclusion that, for the same synthesis temperature, lower quantities of entanglements are produced by a slurry process. According to the above-mentioned model, a possible explanation can be provided by the different effects that temperature and pressure changes have upon the polymerization and crystallization rates in the gas and in the liquid phase, respectively. Synthesis rate is thought to be controlled mostly by the diffusion of the monomer toward the catalyst active site.[41] Thus, the monomer diffusion coefficients have been computed for different combinations of synthesis conditions in the slurry and in the gas phase. Results of computations, performed according to methods reported in the literature,[43] show that synthesis conditions for the Gp85 samples lead to a threefold increase in the monomer diffusion coefficient as compared to gas-phase synthesis at 30 °C. In contrast, in the slurry process, only a twofold increase in the diffusion coefficient is obtained when synthesis conditions are changed from Sl30 to Sl85. Thus, larger increases in the polymerization rate should be obtained for the gas-phase synthesis as temperature is increased from 30 to 85 °C. Effects of temperature and pressure changes on the crystallization rate should be evaluated by an analogous procedure. However, no simple method is available to compute the diffusion coefficient of the polymer segments during the synthesis process. Nonetheless, consideration of the temperature effects on the viscosity of the monomer gas and of the slurry solution can provide qualitative estimates of the changes in the crystallization rate in these two environments. Viscosities of gases increase as temperature is increased.[43] In contrast, liquid viscosity decreases as temperature is increased. Thus, decreasing the viscosity of the slurry solution around the growing crystallites should increase the reptation rate of chain segments onto the crystallite surface. According to Wunderlich,[40,41] chances for entanglement formation become higher when polymerization rate is higher than the rate of crystallization. It can be concluded that comparatively larger increases in the polymerization rate are obtained in the gas phase when synthesis conditions are changed from Gp30 to Gp85. Likewise, decreases in the crystallization rate are lower for the slurry process as temperature is increased. Thus, synthesis in the gas phase should favor formation of entanglements and should therefore decrease powder ductilities, as compared to slurry synthesis at the same temperature.

Conclusions

SAXS investigations on specimens obtained at each step of the draw route provide information on the structural changes associated with the conversion of nascent reactor powders into fibers. Equatorial SAXS patterns show no detectable interference effects. Results of the iterative generalized Guinier analysis on these patterns are consistent with the conclusion that the fiber obtained upon draw of reactor powders is made up by bundle-like fibrillar clusters of different diameters (Table 2 and Figure 3).

In contrast, interference peaks are a characteristic feature of the SAXS meridional profiles. Along the draw route, fibers display the first evidence of interferential effects, which could not be detected in the corresponding nascent reactor powders and in their sintered plates.[14] The absence of interferential effects in nascent powders has been often attributed to chain-extended crystals.[42] However, previous measurements of the crystallite thicknesses by DSC and Raman LAM excluded any significant presence of chain-extended crystals.[10,11] It was concluded that the absence of interference effects in nascent reactor powders should be attributed to the disordered arrangement of crystallites, resulting from irregular stacking of lamellar crystals.[14,44] Only a large reorganization of the crystal macrodomain, as obtained on draw, seems able to improve lamellar stacking regularity at a level that SAXS interference peaks can be detected.

Peak profile analysis has provided quantitative correlations between peak parameters and sample ductility. According to Peterlin's model of drawing,[16,17] higher peak intensities correspond to lower contents of taut tie molecules. The correlation between peak integrated intensities and TDR_{max}, reported in Figure 4, shows that, under similar processing conditions and for the same degree of extension, samples synthesized by a slurry process at 85 °C have lower amounts of taut tie molecules. It can be concluded that synthesis conditions control the most important characteristics of the interphase, including those molecular arrangements which determine the amount of tie molecules.

Additional information on the type and entity of molecular draw is given by the relationships between peak fwhm and TDR_{max}. The fwhm values provide an estimate of the coherency of the lamellar stacking. As reported in Figure 6, TDR_{max} increases regularly as fwhm is increased and samples obtained in different synthesis conditions group neatly along the correlation line. Synthesis by a slurry process at 85 °C can lead to lower amounts of tie molecules. This set of synthesis conditions provides more drawable powders as proved by the higher values of TDR_{max} in Table 1.

Likewise Raman studies show smaller interphase contents of reactor powder,[12] corresponding to less strained intercrystalline layers. Both experiments lead to the conclusion that, after coextrusion, lower amounts of strained chain arrangements in the intercrystalline layers result in higher values of TDR_{max}.

Draw experiments on the reactor powders investigated in this work provide a correlation between higher synthesis temperature and higher ductilities which does not agree with Wunderlich's principles for crystallization on synthesis. Additional features should be introduced in this model to account for such conflicting results. The molecular arrangements stemming from different crystallization dynamics as the synthesis parameters are changed must be considered. The latent entanglement model, presented in the companion paper,[45] seems able to provide satisfactory explanations for the reported dependence of reactor powders ductilities on synthesis conditions.[46]

Acknowledgment. This work was partially supported by the C.N.R., Progetto Strategico "Tecnologie Innovative", and by the Ministero per l'Università e la Ricerca Scientifica e Tecnologica (MURST). The authors are much indebted to Prof. Tetsuo Kanamoto for the important and useful observations advanced upon reading the manuscript. Appreciation is expressed to the NSF MRSEC at UMass for utilization of shared facilities.

References and Notes

(1) Smith, P.; Lemstra, P. J. *Makromol. Chem*. **1979**, *180*, 2983.
(2) Zachariades, A. E.; Watts, M. P. C.; Kanamoto, T.; Porter, R. S. *J. Polym. Sci., Polym. Lett. Ed.* **1979**, *17*, 485.
(3) Smith, P.; Lemstra, P. J.; Booij, H. C. *J. Polym. Sci., Polym. Phys. Ed*. **1981**, *19*, 877.
(4) Smith, P.; Lemstra, P. J.; Kalb, B.; Pennings, A. J. *Polym. Bull*. **1979**, *1*, 733.
(5) Kanamoto, T.; Tsuruta, A.; Tanaka, K.; Takeda, M.; Porter, R. S. *Polym. J*. **1983**, *15*, 327.
(6) Kanamoto, T.; Ohama, T.; Tanaka, K.; Takeda, M.; Porter, R. S. *Polymer* **1987**, *28*, 1517.
(7) Rotzinger, B. P.; Chanzy, H D.; Smith, P. *Polymer* **1989**, *30*, 1814.
(8) Ohta, T.; Wachi, T.; Nagai, T.; Takada, A.; Ikeda, Y.; Ohtsubo, T.; Kawaguchi, A. *Polymer* **1993**, *34*, 4863.
(9) Zachariades, A. E.; Watts, M. P. C.; Porter, R. S. *Polym. Eng. Sci.* **1980**, *20*, 555.
(10) Ottani, S.; Porter, R. S. *J. Polym. Sci., B: Polym. Phys.* **1991**, *29*, 1179.
(11) Wang, L. H.; Ottani, S.; Porter, R. S. *J. Polym. Sci., B: Polym. Phys.* **1991**, *29*, 1189.
(12) Wang, L. H.; Porter, R. S.; Stidham, H. D.; Hsu, S. L. *Macromolecules* **1991**, *24*, 5535.
(13) Strobl, G. R.; Hagedorn, W. *J. Polym. Sci., Polym. Phys. Ed*. **1979**, *16*, 1181.
(14) Ottani, S.; Ferracini, E.; Ferrero, A.; Malta, V.; Porter, R. S. *Macromolecules* **1995**, *28*, 2411.
(15) Hosemann, R.; Bagchi, S. N. *Direct Analysis of Diffraction by Matter;* North-Holland Publishing Co.: Amsterdam, 1962.
(16) Peterlin, A. *Colloid Polym. Sci.* **1987**, *265*, 357.
(17) Peterlin, A. *Polym. Eng. Sci.* **1978**, *18*, 488.
(18) Gibson, A. G.; Davies, G. R.; Ward, I. M. *Polymer* **1978**, *19*, 683.
(19) Prevorsek, D. C.; Harget, P. J.; Sharma, R. K.; Reimscheussel, A. C. *J. Macromol. Sci., Phys.* **1973**, *B8*, 127.
(20) Fischer, E. W.; Goddard, H. *J. Polym. Sci.* **1969**, *C16*, 4405.
(21) Clark, E. S.; Scott, L. S. *Polym. Eng. Sci.* **1974**, *14*, 682.
(22) Wang, L. H.; Ottani, S.; Porter, R. S. *Polymer* **1991**, *32*, 1776.
(23) Vonk, C. G. *J. Appl. Crystallogr.* **1971**, *4*, 340.
(24) Bonart, R.; Hosemann, R. *Kolloid Z. Z. Polym.* **1962**, *186*, 16. See also: Alexander, L. E.; *X-Ray Diffraction Methods in Polymer Science*; John Wiley & Sons: New York, 1969; pp 429−433.
(25) Guinier, A. *Théorie et Technique de la Radiocristallographie;* Dunod: Paris, 1956; pp 644−660.
(26) Vonk, C. G. *J. Appl. Crystallogr.* **1975**, *8*, 340.
(27) Guinier, A.; Fournet, G. *Small Angle Scattering of X-Rays*; John Wiley & Sons: New York, 1955**.**
(28) Porod, G. *Kolloid Z.* **1951**, *124*, 83.
(29) Reinhold, C.; Fischer, E. W.; Peterlin, A. *J. Appl. Phys.* **1964**, *35*, 71.
(30) Peterlin, A. *J. Polym. Sci.: Part C, Polym. Rev.* **1965**, *9*, 1.
(31) Kavesh, S.; Schultz, J. M. *J. Polym. Sci, Part A-2* **1971**, *9*, 85.
(32) (a) Tsvankin, D. Ya. *Polym. Sci. USSR* (*Engl. Transl.*) **1964**, *6*, 2304. (b) Tsvankin, D. Ya. *Polym. Sci. USSR* (*Engl. Transl.*) **1964**, *6*, 2310.
(33) Mutter, R.; Stille, W.; Strobl, G. *J. Polym. Sci., B: Polym. Phys.* **1993**, *31*, 99.
(34) Alexander, L. E. *X-Ray Diffraction Methods in Polymer Science;* John Wiley & Sons: New York, 1969; pp 332−350.
(35) Peterlin, A.; Corneliussen, R. *J. Polym. Sci, Part A-2* **1968**, *6*, 1273.
(36) Hindeleh, A. M.; Johnson, D. J. *Polymer* **1972**, *13*, 423.
(37) (a) Brady, J. M.; Thomas, E. L. *J. Mater. Sci.* **1989**, *24*, 3311. (b) Brady, J. M.; Thomas, E. L. *J. Mater. Sci.*, **1989**, *24*, 3319.
(38) Brady, J. M.; Thomas, E. L. *Polymer* **1989**, *30*, 1615.
(39) Adams, W. W.; Briber, R. M.; Sherman, E. S.; Porter, R. S.; Thomas, E. L. *Polymer* **1985**, *26*, 17.
(40) Wunderlich, B. *Macromolecular Physics, 2*; Academic Press: New York, 1976; pp 271−327.
(41) Muñoz-Escalona, A.; Parada, A. *Polymer* **1979**, *20*, 859.
(42) Smith, P.; Chanzy, H. D.; Rotzinger, B. P. *J. Mater. Sci.* **1987**, *22*, 523.
(43) (a) Bird, R. B.; Stewart, W. E.; Lightfoot, E. N. *Transport Phenomena*; Wiley: New York, **1960** Chapter 16. (b) Reid, R. C.; Prausnitz, J. M.; Poling, B. E. *The Properties of Gases and Liquids*; McGraw-Hill: New York, 1988; Chapter 11.
(44) Tervoort-Engelen, Y. M. T.; Lemstra, P. *J. Polym. Commun.* **1991**, *32*, 343.
(45) Ottani, S.; Ferracini, E.; Ferrero, A.; Malta, V.; Porter, R. S. "A Latent Entanglement Model: Effect of Irregularities of the Crystallite Fold Surface in the Draw of Semicrystalline High Polymers", submitted.
(46) Ottani, S.; Porter, R. S. *Macromol. Rapid Commun.* **1995**, *16*, 813.

MA951264M